Article:
Borah, PK, Rappolt, M, Duary, RK et al. (1 more author) (2019) Structurally induced modulation of in vitro digestibility of amylopectin corn starch upon esterification with folic acid. International Journal of Biological Macromolecules, 129. pp. 361-369. ISSN 0141-8130

https://doi.org/10.1016/j.ijbiomac.2019.02.051

Accepted Manuscript

Structurally induced modulation of in vitro digestibility of amylopectin corn starch upon esterification with folic acid

Pallab Kumar Borah, Michael Rappolt, Raj Kumar Duary, Anwesha Sarkar

PII: S0141-8130(18)36827-2
DOI: https://doi.org/10.1016/j.ijbiomac.2019.02.051
Reference: BIOMAC 11704

To appear in: *International Journal of Biological Macromolecules*

Received date: 8 December 2018
Revised date: 7 February 2019
Accepted date: 8 February 2019

Please cite this article as: P.K. Borah, M. Rappolt, R.K. Duary, et al., Structurally induced modulation of in vitro digestibility of amylopectin corn starch upon esterification with folic acid, International Journal of Biological Macromolecules, https://doi.org/10.1016/j.ijbiomac.2019.02.051

Structurally induced modulation of in vitro digestibility of amylopectin corn starch upon esterification with folic acid

Pallab Kumar Borah [a, b], Michael Rappolt [a], Raj Kumar Duary [b]†, Anwesha Sarkar [a]*

[a] Food Colloids and Processing Group, School of Food Science and Nutrition, University of Leeds, LS2 9JT, United Kingdom

[b] Department of Food Engineering and Technology, School of Engineering, Tezpur University, 784 028, India

***Corresponding author:**

Dr. Anwesha Sarkar, E-mail address: A.Sarkar@leeds.ac.uk

†Joint corresponding author

Dr. Raj Kumar Duary, E-mail address: duary@tezu.ernet.in, rkduary@gmail.com

Abstract

The present study aims to identify how structural modifications of amylopectin corn starch on esterification with folic acid (FA) affects its in vitro digestion. Small angle X-ray scattering (SAXS) confirmed that at low FA esterification (5-10%), the mesophase order showed the absence of any super-structural order. However, a discotic stacking of SF forming columnar hexagonal phases and columnar helical phases (with strong optical anisotropy) was observed upon increasing FA esterification (20-40%). X-ray diffraction (XRD) evidenced the development of a V and B-type molecular packing order in SF with increased FA esterification from 20-40%, with a consequential increase in the percentage of slow digestible starch (SDS) and resistant starch (RS). The slower digestion phenomenon displayed a dual-phase behavior, with digestion rates $k_1 > k_2$, where k_2 being ca. 0.3 of k_1. Stacking over packing order appeared to be more influential in limiting the enzymatic action. A k-means clustering analysis of the total digested starch and Fourier transform infrared (FTIR) spectroscopy peak ratios (1000/1022) cm^{-1} indicated that 0.04 level FA substitution was crucial for slower hydrolysis of SF. This study provides structural insights for developing starch-folic acid ester derivatives that could form building-block copolymers for future development of oral drug/ nutraceutical delivery vehicles with tailored starch digestion properties.

Keywords

Starch; folic acid; esterification; structure; digestion; SAXS.

1. Introduction

Starch is recognized as one of the most promising building-block polymers for designing biocompatible oral drug delivery systems for a therapeutic utility in chronic gastrointestinal diseases, including inflammation and cancers [1]. In particular, starch has received much attention in this area due to its abundant availability, low-cost, biodegradability, biocompatibility, and non-toxicity. Moreover, starch itself is a physiologically active component. Modified starches have been shown to ameliorate the conditions of colon cancer, lower cholesterol and reduce cardiovascular diseases [2].

Starch has recently been explored for the preparation of relatively inexpensive drug delivery systems with the capability of molecular recognition of inflamed and cancerous cells inside mammalian systems via esterification of folic acid (FA), the latter is a water-soluble vitamin. In particular, FA is widely accepted as a ligand molecule for targeted cancer therapies as compared to other water-soluble vitamins. This is because FA specifically binds with its high binding affinity, $K_d \sim 10^{-10}$ M to folate receptors [3-5], that are overexpressed in various epithelial cancers, such as brain, breast, colorectal, renal, nasopharyngeal, ovarian, and uterine [6]. However, such esterification of starch-based delivery systems using FA has been demonstrated to result in multi-scale structural modifications [3, 4, 6]. Starch is structurally arranged in granules (~1-100 µm in size) which are partly crystalline in nature and consist of alternating layers of amorphous and semi-crystalline domains. These semi-crystalline domains can again be described as a lamella formed by amorphous and crystalline regions with repeat distances ranging 9-10 nm [7]. During the esterification process with FA, there are intermediate steps that involve treatment with solvents (e.g. dimethyl sulfoxide (DMSO)). In a recent study, it was demonstrated that such intermediate steps result in profound mesoscopic structural

rearrangements in starches [5]. A loss of 75% of the semi-crystalline registries of amylopectin corn starch (corresponding to a repeat distance of ca. 9 nm) upon initial DMSO treatment was observed, followed by the total loss of stacking and packing order in the starches upon treatment with the cross-linker, n, n'-dicyclohexylcarbodiimide (DCC) [5]. Upon esterification with FA, an FA-assisted self-assembly and cross-linking of starch-folic acid ester (SF) derivatives was postulated, which resulted in the development of discotic stacking of SF forming hexagonal columnar phases (lattice parameter of ca. 4.5 nm) [5]. However, how the structure of starch may evolve over a range of degree of substitutions with FA remains poorly understood.

More importantly, starch-based delivery systems can be eroded by amylases in the oral and intestinal phases after ingestion, restricting their abilities for the site-dependent release of the drug/ nutraceutical when administered via the oral route. Recently, it has been shown that folic acid can inhibit the catalytic efficiency of α-amylase [8]. Therefore, it can be hypothesized that esterification of starch with folic acid could modulate the digestion of these SF delivery systems within the gastrointestinal system. However, the role of structural modification of starch upon creation of SF esters on starch digestion kinetics has not been reported to date. Understanding the structural mechanism behind altered digestion of starch on esterification with FA is key to design SF esters with dual benefits of, (a) resisting digestion to allow the site-dependent delivery of the drug/nutraceutical and (b) capability of FA for high-affinity targeting and molecular recognition of folate receptors in cancer cells.

Therefore, the present study aims to understand the evolution of the hierarchical mesoscopic structure within SF on a progressive increase in FA substitution and investigate how this affects the digestion kinetics. To understand the structural mechanism behind the digestion behavior, a combination of complementary techniques of scattering (small-angle X-ray scattering), diffraction (XRD), Fourier transform infrared (FTIR) spectroscopy, microscopy

(bright-field and polarized, scanning electron), and in vitro digestion (classical Englyst digestion and kinetics) were employed. Amylopectin corn starch was used in this study as it is the major constituent of widely utilized cereal starches, and consequently, it is the main substrate for digestion by α-amylase [9]. However, studies on the impact of amylopectin internal molecular structure on starch digestibility have been scarce to date [10]. Additionally, amylopectin corn starch lacking amylose has recently been acknowledged as a good structural model within starch [10]. The internal regions of amylopectin form amorphous lamellae whereas the external regions form crystalline phases. Noteworthy, any change in these clearly defined structural aspects of amylopectin on esterification by FA can be straightforwardly identified by applying X-ray scattering techniques. To our knowledge, this is the first study that demonstrates the structural mechanism behind the digestion behavior of SF esters.

2. Materials and Methods

2.1. Materials

Pepsin from porcine gastric mucosa (3200-4500 U mg^{-1}), pancreatin from porcine pancreas (4 × USP), α-amylase type VI-B from porcine pancreas (> 10 U mg^{-1}), amyloglucosidase from Aspergillus niger (> 70 U mg^{-1}), invertase from baker's yeast (Saccharomyces cerevisiae) (> 300 U mg^{-1}), amylopectin corn starch (ACS), folic acid (FA), n, n'-dicyclohexylcarbodiimide (DCC), 4-dimethylaminopyridine (DMAP), dimethyl sulphoxide (DMSO) were purchased from Sigma-Aldrich, India. Milli-Q water (Milli-Q apparatus, Millipore Corp., USA) was used throughout the experiments.

Starch folic-acid (SF) esters with different degrees of substitution of FA were synthesized as described previously [5]. Briefly, FA was reacted with DCC and DMAP (FA: DCC: DMAP

molar ratio of 1:1:0.3) by stirring for 30 min in DMSO. ACS was added to the reaction mixture (5-40 wt% of FA to starch dry weight) and was further reacted under dark conditions for 24 h. The reactions were carried out at 30 ºC. The reaction products were washed with 0.1 M HCl and water, and then dialyzed (3.5 kDa MWCO) against 10 mM phosphate buffer at pH 7.4 containing 0.10 M NaCl for 24 h, and, then with water for another 24 h, to remove any unbound FA and traces of DCC and DMAP. The product was lyophilized, ground to a fine powder, and the SF ester derivatives (SF5, SF10, SF20, SF30, and SF40) were obtained. Evidence of the esterification between ACS and FA is described previously using confocal laser scanning microscopy [5]. The degree of substitution of FA via the esterification reaction is described previously using spectroscopy as follows, SF5: 0.01, SF10: 0.02, SF20: 0.04, SF30: 0.05 (sample: degree of substitution (the number of FA per glucose residues of ACS) [5]. Using the previously described methods [5], the degree of substitution of SF40 was estimated as 0.07 and **Fig. S1** shows the confocal micrograph.

The control groups were: ACS, ACS treated with DMSO (S/DMSO) and ACS treated with DMSO and DCC/DMAP (S/DCC). Additional controls included, S/DMSO mixed with 20 and 40 wt% of FA to starch dry weight, i.e., $SF20_{unesterified}$ and $SF40_{unesterified}$, respectively.

2.2. Small-angle X-ray scattering (SAXS)

The SAXS instrument setup (SAXSpace, Anton Paar, Austria) used in this study is described in detail elsewhere [11, 12]. Sample preparation, experimental conditions and the data manipulation have been described previously [5]. The structural parameters from the SAXS data (0.1 $nm^{-1} < q < 2.5$ nm^{-1}) were obtained by fitting to a Cauchy-Lorentz-Power Law equation [5, 13] as shown in equation (1),

$$I(q) = I_{max}\left[1 + \left(\frac{2(q-q_{\max})}{\Delta q}\right)^2\right]^{-1} + Aq^{-\delta} \quad (1)$$

where A, δ, I_{max}, q_{max}, and, Δq (FWHM) are adjustable positive parameters.

A model for stacked discs was implemented for one of the samples. Briefly, the scattered intensity I(q) is calculated [14] as in equation (2),

$$I(q) = N \int_0^{\pi/2} [\Delta\rho_t\{V_t f_t(q,\alpha) - V_c f_c(q,\alpha)\} + \Delta\rho_c\{V_c f_c(q,\alpha)\}]^2 S(q,\alpha) \sin\alpha \, d\alpha + I_b \quad (2)$$

where the contrast, $\Delta\rho_i = \rho_i - \rho_{solvent}$, I_b was the background, and N was the number of discs per unit volume (the total number of the disks stacked per unit was set to 1).

Silver behenate with a known lattice spacing of 5.84 nm was used to calibrate the scattering vector q as, $q = \frac{4\pi}{\lambda} sin\theta$, where λ = 0.154 nm and 2θ is the scattering angle.

2.3. X-ray diffraction (XRD)

The XRD data (angular range, 2θ = 10-30°) of the dry samples were recorded at room temperature (25 °C) on a D8 Focus X-ray diffractometer (Bruker AXS, Germany) using Cu Kα (λ = 0.154 nm) radiation. A small quantity of the sample was mounted on an aluminum sample holder and leveled with a glass slide. Note, the scattering vector q is defined equally as in section 2.2.

The spectra were baseline corrected using OriginPro 8.0 (OriginLab Corp, USA), and, the relative crystallinity (X_c, %) was calculated according to equation (3),

$$X_c = \frac{\sum_{i=1}^{n} A_{ci}}{A_t} \quad (3)$$

where A_{ci} is the area under each crystalline peak with index i; and A_t is the total area of the diffraction pattern.

2.4. Polarized light microscopy

A Motic BA310Pol polarization microscope (Motic, Hong Kong) was used at 400x magnification for imaging of the sample. Bright-field micrographs were obtained in the same set-up, without

crossed-polarizers. Suspension of 0.5% (w/v) samples were prepared as a wet film on a glass slide before imaging.

2.5. Scanning electron microscopy (SEM)

Scanning electron micrographs were obtained on a JSM 6390 LV (JEOL, Singapore) microscope. A suspension of 0.5% (w/v) sample was prepared as a wet film on a glass slide (thickness, 0.16 mm) and then dried under nitrogen. The sample was then sputter-coated with platinum and imaged at an accelerating voltage of 20 kV.

2.6. Fourier transform infrared spectroscopy (FTIR)

The FTIR spectra (1200-800 cm^{-1}) of the samples were obtained on a Bruker ATR-FTIR Spectrometer (Bruker Optics GmbH, Germany). Baseline correction was performed using anchor points at 1200 and 800 cm^{-1}, followed by interpolation. The peaks at 1022 and 1000 cm^{-1} were selected and Lorentz peak fitting was performed using OriginPro 8.0 (OriginLab Corp, USA).

2.7. Degree of starch hydrolysis

In vitro digestion was carried out as using a method described earlier [15], with some modifications. Briefly, 100 mg samples were used for each experiment and mixed with α-amylase (75 U mL^{-1}) and $CaCl_2$ (0.75 mM) solution for 5 min at 37 °C to replicate oral phase digestion. This was followed by the addition of the simulated gastric fluid containing 0.26 g L^{-1} KCl, 0.06 g L^{-1} KH_2PO_4, 1.05 g L^{-1} $NaHCO_3$, 1.38 g L^{-1}NaCl, 0.12 g L^{-1} $MgCl_2(H_2O)_6$, 0.02 g L^{-1} $(NH_4)_2CO_3$ and 1.02×10^4-1.40×10^4 U mL^{-1} pepsin, pH of the solution was adjusted to 2.20 ± 0.05. Although the study focused primarily on the digestion of SF, pepsin was used at this stage, as starches contain small quantities of proteins, which may interfere with amylase digestion. The simulated gastric digestion was carried out for 30 min.

Simulated intestinal digestion was initiated by adding simulated intestinal fluid containing 0.25 g L^{-1} KCl, 0.05 g L^{-1} KH_2PO_4, 3.57 g L^{-1} $NaHCO_3$, 1.12 g L^{-1} NaCl, 0.33 g L^{-1}

$MgCl_2(H_2O)_6$, 0.44 g L^{-1} $CaCl_2.2H_2O$, 0.23 g L^{-1} bile salts, 0.12 g mL^{-1} pancreatin (lipase activity: > 8 U mg^{-1}, amylase activity: > 100 U mg^{-1}, protease activity: > 100 U mg^{-1}) and 0.21 U mL^{-1} amyloglucosidase and 0.90 U mL^{-1} invertase (pH of the solution was adjusted to 6.80 ± 0.05). The pH was maintained during the digestion process by the addition of HCl and NaOH, as necessary.

The glucose content was analyzed in the supernatants (0.5 mL), collected during simulated gastric and intestinal digestion. To stop the enzymatic reactions, neutralization of pH in the gastric phase was performed by adding 0.5 M sodium bicarbonate, and the samples were then snap-frozen at -20 °C following the intestinal phase. The release of glucose equivalent was monitored using the dinitrosalicylic acid (DNSA) method at 575 nm [16]. To estimate the quantity of hydrolyzed starch, a factor of 0.9 was multiplied by the glucose content [17]. The percentage of hydrolyzed starch (glucose equivalent released) was calculated as in equation (4),

$$Starch\ hydrolysis\ \% = \frac{S_h}{S_i} = 0.9 \times \frac{G_p}{S_i} \quad (4)$$

where S_h is the amount of hydrolyzed starch, S_i is the initial amount of starch, and G_p is the amount of glucose produced. The fractions of starch (%), i.e., readily digestible starch (RDS), slow digestible starch (SDS), and resistant starch (RS) were estimated as described previously [18].

2.8. Kinetics

Starch hydrolysis rate constants were measured using a method described previously [19, 20], which is an improvisation of the Guggenheim approach to events in which the intervals (Δt) amidst measurements are not constant. Under ideal conditions, a first-order equation [17] describes the digestibility of starch as shown in equation (5),

$$C_t = C_\infty(1 - e^{-kt}) \quad (5)$$

where C_t is the product concentration, with a certain degree of hydrolysis at time t. C_∞ is the proportional end point concentration representing the total digested starch, and k is the first-order rate constant of digestion. Differentiating C_t by time and then expressing equation (6) in the logarithmic form gives,

$$\ln\left(\frac{dC}{dt}\right) = \ln(C_\infty k) - kt \quad (6)$$

Therefore, from equation (6), the plot of $\ln\left(\frac{dC}{dt}\right)$ against t represents a linear relationship with a slope of -k. Here, the y-intercept of the plot is equal to $\ln(C_\infty k)$, therefore, the value of k can be estimated from the slope. This is described as the logarithm of the slope (LOS) plot. The slope of a digestibility curve at different time points was evaluated from the quantity ΔC as, C_t of two successive events over the difference of corresponding hydrolysis time (t) events. The natural logarithms of this quantity were plotted against the mean of the corresponding time.

As in vitro digestion proceeds asymptotically, the value of ΔC approaches zero; therefore, later estimates were excluded from LOS and interpreted as resistant starch (RS). During a digestion reaction, the slope (of the linear fit) is highly sensitive to changes in the value of k. This could show as disjointedness in the linear plot. The point of intersection of the disjointed linear plots reveals us the distinction point between readily digestible starch (RDS) and slow digestible starch (SDS). The fit with a steeper linearity was considered as RDS, and the latter fit was considered as the SDS region.

2.9. Statistical analysis

The Cauchy-Lorentz-Power Law model for the samples SF5, SF10, SF20, and SF30 were implemented in Matlab R2015b (The MathWorks, Inc., USA). The stacked disc model for the sample SF40 was implemented in SASView 4.1.2. An unsupervised k-means clustering method

[21] using the city block distance metric was implemented in Matlab R2015b (The MathWorks, Inc., USA). The data (FTIR peak ratio (1000/1022) cm^{-1} and C_∞ (%) data from the samples) was partitioned into k clusters (k = 2) which were mutually exclusive. Initially, each such cluster comprised of a randomly placed centroid. The sum of distances from all member data points in such clusters is minimized from the centroid and the latter updated until convergence. Analysis of variance (ANOVA) and Tukey's HSD Post Hoc analyses were conducted using SPSS 8.0 (SPSS, Inc., USA). Treatment means were considered significantly different at $p < 0.05$.

3. Results and Discussion

Firstly, the characterization of folic acid (FA) esterified amylopectin corn starch (ACS) will be discussed. We especially focus on the evolution of the structure of starch-folic acid ester (SF) derivatives, as it sets the scene for understanding the digestion behavior of these esterified systems.

3.1. Mesoscopic structure

The quasi-long-range mesoscopic order of the samples, namely SF5, SF10, SF20, SF30, and SF40, profoundly altered due to esterification with FA of increased concentrations as characterized by SAXS (**Fig. 1a**). All data were fitted using the Cauchy-Lorentz-Power Law model, described in equation (1). A total absence of any structure factor contribution was observed for SF5 and SF10 (**Fig. 1a**: orange, '○' and red, '△'), indicating the absence of any super-structural order and comprised of disordered random SF polymer derivatives. For the sample SF20 and SF30 (**Fig. 1a**: blue, '▽', and, magenta, '□'), a characteristic peak at ca. 1.60

nm^{-1}, corresponding to the repeat distance of ca. 3.92 nm (note, d = $2\pi/q$) was observed. This process of FA-assisted self-assembly in FA derivatives (including FA derivatives of starch) and the subsequent formation of discotic liquid crystals forming hexagonal columnar phases with a lattice parameter of ca. 4.7 nm, corroborates previous findings [5, 22, 23]. In the present study, self-organization in SF20 and SF30 was found to be concentration dependent, with the first order d_{10} lattice spacing of 3.84 and 4.02 nm (corresponding unit cell lattice parameters $a = 2/\sqrt{3} \cdot d_{10} =$ 4.43, and 4.64 nm, respectively).

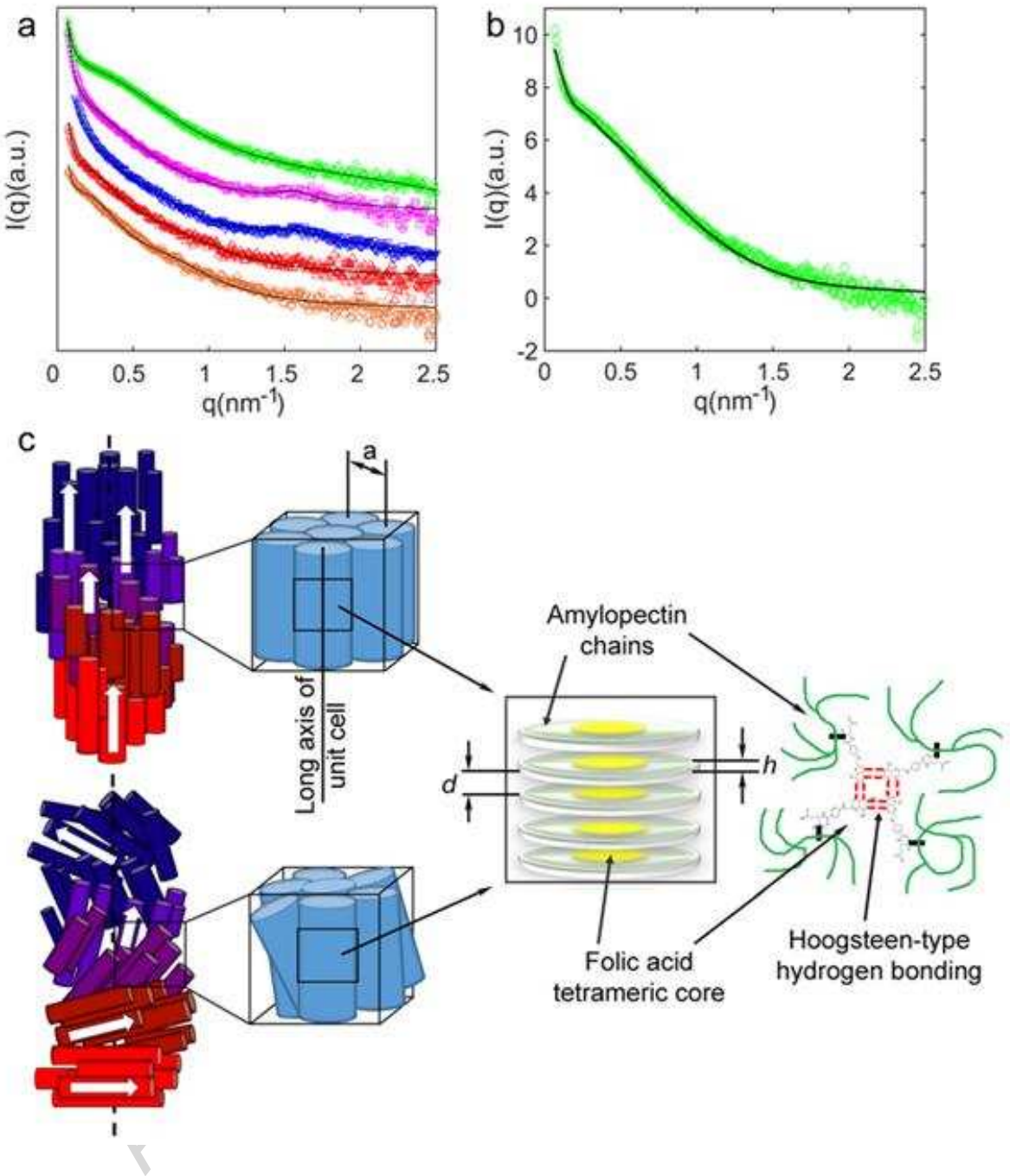

Fig. 1. Background subtracted SAXS curves ($0.1 < q < 2.5$ nm^{-1}). Cauchy-Lorentz-Power law model function fits (solid line, equation (1)) of SF5-SF40, data have been shifted vertically for clarity (a), SF40 fitted to the stacked disc model (solid line, equation (2)) (b), and scheme depicting the supramolecular arrangement of the SF tetrameric assemblies for SF20-SF30 (left, top) and SF40 (left, bottom) (c). Here, a = hexagonal lattice parameter, h = core thickness, and, d = layer thickness. Legends represent, SF5 (orange, 'o'), SF10 (red, '∆'), SF20 (blue, '▽'), SF30 (magenta, '□') and SF40 (green '◊').

Notably, for SF40 (**Fig. 1a,** cf. green '◊'), the peak around ca. 1.60 nm^{-1} was no longer observed, indicating a loss of hexagonal arrangement of columnar phases (unit cells). Rather, a broad scattering contribution ranged ca. $0.15 < q < 0.85$ nm^{-1} in the intermediate q regime was apparent. Spacing corresponding to this broad scattering contribution ranged from about 8-41 nm. This increase in scattering contribution in the intermediate q region of SAXS is in agreement with previous reports on retrograded potato and corn starch, propionylated starches, starches plasticized with triacetin, and starches treated with hydrothermal and hydrostatic pressure [24-28].

The fit from the Cauchy-Lorentz-Power Law model, estimated the q_{max} for the scattering contribution to be 0.23 nm^{-1}, which corresponds to a *D*-spacing of 27 nm. This is 6-7 times larger in comparison to the former samples SF20 and SF30, and hence unlikely to be stemming from the arrangement of unit cells (**Fig. 1c**, left-hand side). Still, SF40 was organised as liquid crystalline mesophase, which builds on the self-assembly of columnar disc-like blocks that have flexible amylopectin chains attached to a (fairly rigid) FA tetramer core (**Fig. 1c**). Such, amylopectin chains accommodated between the stacked discs can cross-link owing to hydrogen bonding amidst chains, leading to the development of a layer of polymer chain packing (new lamellar arrangement) resulting in an increased *D*-spacing. Presence of such large D-spacing has been observed previously in retrograded corn and potato starches [27]. This broad Bragg peak contribution ($q = 0.2$-0.4 nm^{-1} corresponding to D-spacing of ca. 31-15 nm) has been assigned to a larger lamellar repeat in the semi-crystalline regions in starch (larger than the conventional ca. 9-10 nm lamellar repeat). Pu and coworkers [28] have pointed towards the formation of repeated stacking lamella after the hydrothermal-pressure treatment of corn starch. They observed the appearance of shoulder-like scattering contribution at $q = 0.35$-0.43 nm^{-1}, corresponding to a D-spacing of ca. 18-15 nm. Therefore, it is plausible that the large D-spacing in SF40 in the present

study is caused by amylopectin chains forming newer lamellar repeat layers amidst discs. Considering this, a model for stacked discs with a core and layer structure was implemented. Briefly, the model estimates the form factor P(q) for stacked discs that comprise a core and layer structure, where P(q) is normalized using the volume of the cylinder. Assuming the D-spacing (D = layer thickness, d, plus core thickness, h; see right-hand side of **Fig. 1c**) in a parallel stack of discs to obey a Gaussian size-distribution, a structure factor S(q) proposed earlier [29] is used in this function (equation (2)). **Fig. 1b** (solid line) shows the fitted stacked disc model. From equation (2) (assuming the scattering arising from fully exfoliated monodisperse disks), the core thickness (h) of the disc was estimated to be 1.2 nm thick followed by an adjacent layer thickness (d) of 29.8 nm (note, the corresponding core plus layer thickness parameter agrees fairly well to the D-spacing in SF40 retrieved from equation (1)). Since, the symmetry of such SF discotic phases are known to be chiral [22, 23], the organization in layers of such molecules could give rise to specific shapes with directionality of alignment, causing a polar order in each of the layers [30]. This polar order and the chirality is known to yield interesting phenomena, such as the spontaneous formation of chiral and helical super-structures [30, 31].

The presence of elongated super-structures forming dense microfibrils with a pronounced directionality was observed in optical micrographs of SF40 (**Fig. 2a**). Note, such fibrillous structures were not observed for the other samples (**Fig. S2**). The elongated super-structures (indicated by arrows) of the wet films in bright-field microscopy were additionally confirmed using scanning electron microscopy on the dehydrated SF40 at a lower length scale (**Fig. 2b, c**). Optical microscopy in combination with crossed-polarizers revealed high optical anisotropy in SF40 (**Fig. 2d-f**), suggesting that the microfibrils were helical. The sample along the major axis appeared to possess a principal linear optical axis. As the sample stage was rotated to 45°, the

bright birefringent domains in the sample darkened (cf. **Fig. 2d** transition to **Fig. 2e**, enclosed within white circles), and vice-versa (dark to bright domain transition enclosed within white squares, cf. **Fig. 2d** transition to **Fig. 2e**). Therefore, corresponding to the plane of vibration of the incident light, the optical axis should be aligned close to parallel. Furthermore, as the angle to the crossed-polarizers was rotated a further to 90°, the darker domains became brighter (cf. **Fig. 2e** transition to **Fig. 2f**, enclosed within white circles), and vice versa (bright to dark domain transition enclosed within white squares, cf. **Fig. 2e** transition to **Fig. 2f**). Thus, corresponding to both the analyzer and the polarizer, the optical axis should be now tilted. This optical occurrence has about 45º periodicity. The video recording (**Video S1**) of SF40 shows real-time birefringence in the microfibril domains transitioning as the sample stage is rotated 360º. All crossed-polarized micrographs (**Fig. 2d-f**) are analogous to the microfibrils observed under bright-field (**Fig. 2a**). Bright and dark domains correspond to the polarized light being disintegrated into fast and slow components that were not in phase with each other. This confirmed that the unit assemblies present in SF40 have a dominant optical axis, which is linear to its long axis, decorated in an anisotropic manner.

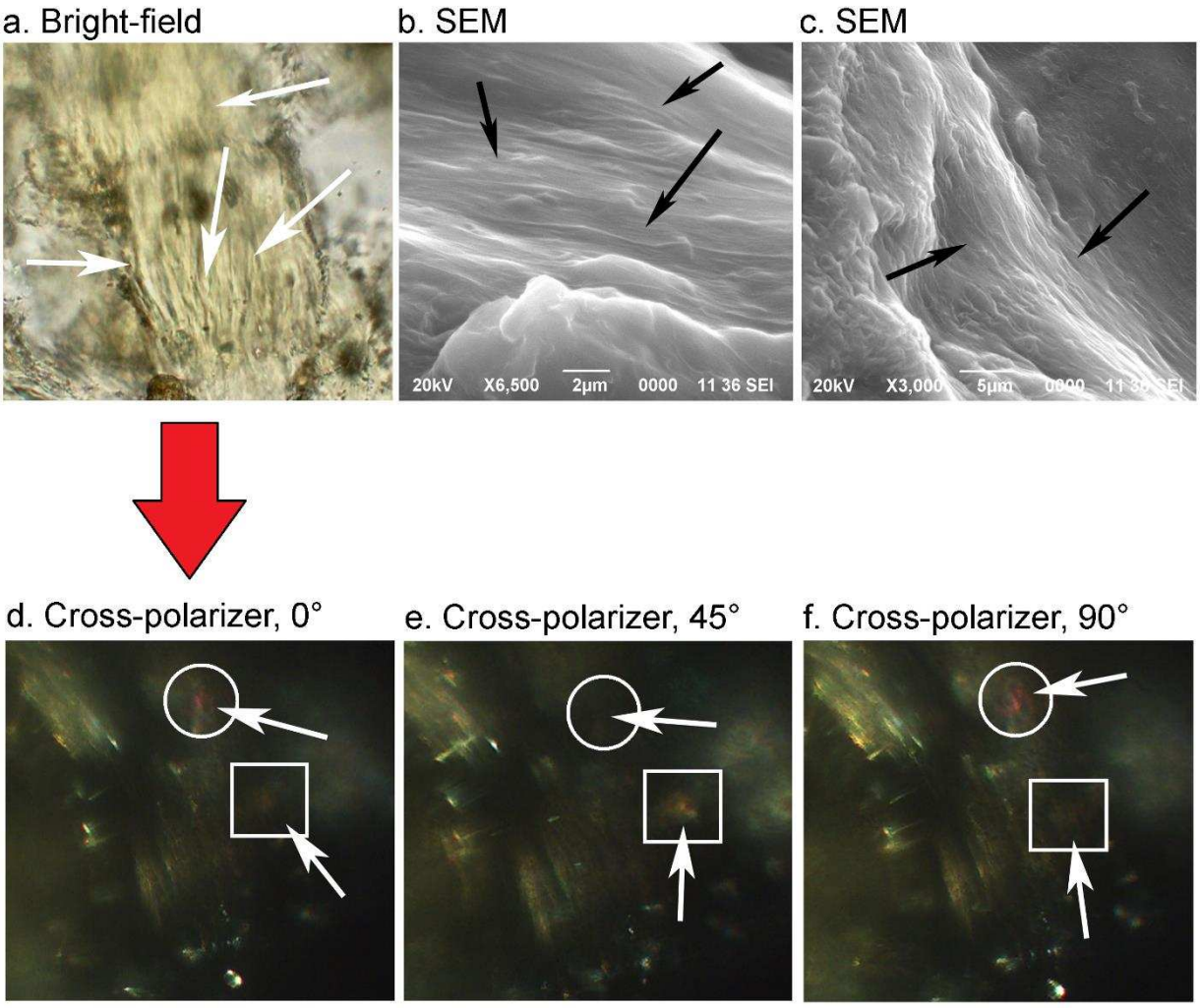

Fig. 2. Optical micrograph of SF40 wet film showing microfibril (marked by arrows) like super-structures under bright-field (a), and scanning electron micrographs of SF40 dry film showing microfibril (marked by arrows) like super-structures (higher magnification, 6,600x (b); lower magnification, 3,000x (c)), micrographs corresponding to the sample position in bright-field microscopy together with crossed-polarizers at 0°, 45°, and 90° showing strong optical anisotropy with bright and dark domains (marked by arrows, outlines indicated by white circle and squares represent identical regions in the various micrographs) of independent alignment (d-f). Rotating the sample stage with a 45° periodicity entirely inverts the domain transmission with respect to the preceding crossed-polarizer micrograph. Image resolution was 400x. **Video S1** (Supplementary file) shows real-time inversion of the domain transmission as the sample stage is rotated 360°.

3.2. Molecular packing and relative crystallinity

X-ray diffraction (XRD) was employed to characterize the SF polymers at spacing < 1 nm evaluating the difference in the packing order. **Fig. 3** exhibits the XRD diffractograms of the samples under study (SF5-SF40). For SF5, no particular crystalline packing order was visible in the diffractograms (**Fig. 3**). The sample SF10 exhibited a broad diffraction contribution centred around 14 nm^{-1} (**Fig. 3**). This is unlike A, B, C, or V-type diffraction commonly observed in starch. Following the entirely disordered SF5 phase, we assume this to be an intermediate state of loose packing preceding the ordered packing in SF20 to SF40. In the samples SF20, SF30, and SF40 (with higher FA esterification), major peaks with q diffraction vector at 5.5 and 14.3, and, 12.3, 15, 15.5 nm^{-1} corresponding to 2θ angles of 7.7º and 20º, and, 17.4º, 21.2º and 22º, respectively, were observed. This is indicative of a V and B-type packing order, respectively [32-34]. The V-type packing order typically associates with the single left-handed helical conformation of starch polymer chains in the presence [7, 35] and also in the absence [36] of low-molecular weight molecules. Additionally, the conformation of B-type packing order comprises a hexagonal packing of right-handed double helices of starch polymer chains [37]. In our case, we propose the packing order to be a polymorph of mixed V and B-type. The control sample, ACS displayed major peaks with scattering vector q at 10.6, 12.0, and 12.6 nm^{-1} (corresponding 2θ angles, 15°, 17°, 18°, and 23°), specific for the A-type monoclinic crystals (**Fig. S3**). The sequence of events that led to the transformation of this A-type to the B-type diffraction pattern upon esterification with higher quantities of FA (as in the case of SF20) is explained more in detail elsewhere [5]. Among other experiments, $SF20_{unesterified}$ and $SF40_{unesterified}$ evidenced major peaks with scattering vector q at ca. 7 nm^{-1} (corresponding 2θ angle, 10°) (**Fig. S3**). Vora and coworkers [38] reported a diffraction peak of FA at 2θ of 10°. Note, in $SF40_{unesterified}$, a secondary diffraction peak with scattering vector q at ca. 9 nm^{-1}

(corresponding *2θ* angle, 13º) emerged (**Fig. S3**). This is indicative of a V-type packing order (helical V-type inclusion complexes), known to form in the presence of low molecular weight ligands such as FA [34]. However, no signs of B-type packing order was observed in either of the unesterified samples. This indicates that an esterification reaction such as DCC/DMAP in the case of the present study is essential for the FA-assisted development of the specific V and B-type diffraction patterns as observed in SF20 and SF40.

The diffractograms were further used to calculate the relative crystallinity (%) of the samples. For SF5 and SF10, we failed to calculate a relative crystallinity. In contrast, the samples SF20, SF30, and SF40 exhibited a relative crystallinity of ca. 19%, 24%, and 25%, respectively. We note, as the samples arise from liquid crystalline mesophases, the chains being fluid should provide the necessary mobility to inhibit the formation of samples with high crystallinity.

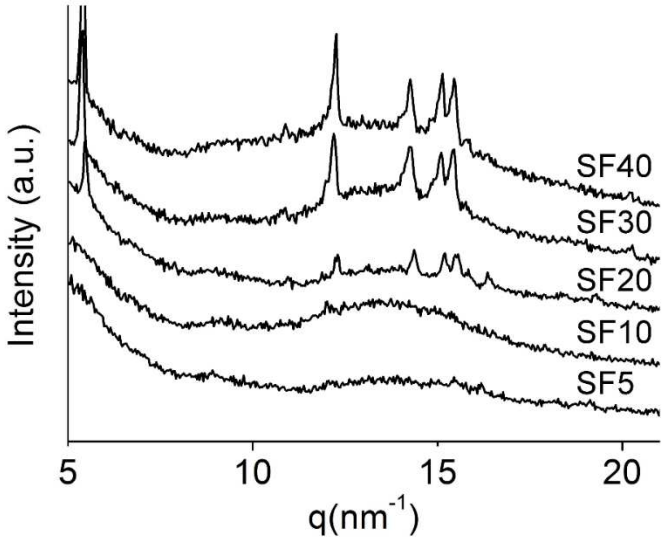

Fig. 3. XRD diffractogram of the samples SF5 to SF40.

In summary, the mesoscopic order of SF was seen to be altered at three stages of FA esterification, i.e., (a) existence of a random chain arrangement at 5-10 wt% FA esterification, (b)

development of discotic stacking of SF forming columnar hexagonal phases at 20-30 wt% FA esterification, and, (c) evolution of discotic stacking of SF forming columnar helical phases at 40 wt% FA esterification. Additionally, the packing order revealed that the evolution of a V and B-type polymorphism, alongside a progressively increasing relative crystallinity in SF20, SF30, and SF40. Since digestion of starch polymer is well-known to be closely related to its structure, we hypothesized that our observations for SF5-SF40 were highly likely to influence their digestion behavior.

3.3. In vitro digestion

The progressive development of discotic stacking, and V and B-type packing order in SF were examined for effects on digestion in an in vitro model. As seen in **Fig. 4a**, an increase in FA substitution resulted in a decrease in readily digestible starch (RDS) and consequent increase in slowly digestible starch (SDS) and resistant starch (RS) content, respectively. In SF5 to SF40, the SDS content significantly increased from 14 ± 1 to 35 ± 1 %, respectively (**Fig. 4a**). Although it is reported that FA inhibits the catalytic efficiency of starch-digesting enzymes, such as α-amylase [8], the increase in SDS content did not show a linear relationship to the degree of FA esterification. This suggests that the hierarchical structural evolution of starch with alternations of the stacking and packing order played an important role in digestion kinetics, which to our knowledge has never been reported earlier in literature. The RDS, SDS, and RS content of the controls, i.e., ACS, S/DMSO, S/DCC, $SF20_{unesterified}$ and $SF40_{unesterified}$ are presented in **Fig. S4a**. The SDS content in the samples roughly corresponds to the loss of 75% of the semi-crystalline registries of amylopectin corn starch upon initial DMSO treatment, as discussed earlier [5]. However, a marked increase in RS content was observed for the samples $SF20_{unesterified}$ and $SF40_{unesterified}$ (**Fig. S4a**). This might be attributed to two synergistic factors, i.e., (a) formation of V-type packing order as observed via XRD (**Fig. S3**) and (b) the ability of FA to inhibit α-

amylase activity [**8**]. Further work is in progress where amylopectin corn starch and folic acid mixtures are being evaluated in order to understand the detailed structural alterations and kinetics of inhibition of the starch digesting enzymes, such as α-amylase and α-glucosidase.

It has been stated previously [39] that the classification of starch into RDS, SDS, and RS is to some extent erroneous because the digestion of processed starch polymer is described by a pseudo first-order reaction process with a single rate constant. Instead, as proposed previously [19, 40], the digestion process can be better understood by employing multiple distinct first-order reactions, carrying independent rate constants. The polymer digestion data was therefore fitted to the first-order kinetic model as described in equation (6) (derived from equation (5)), applying the logarithm of the slope (LOS) plot method.

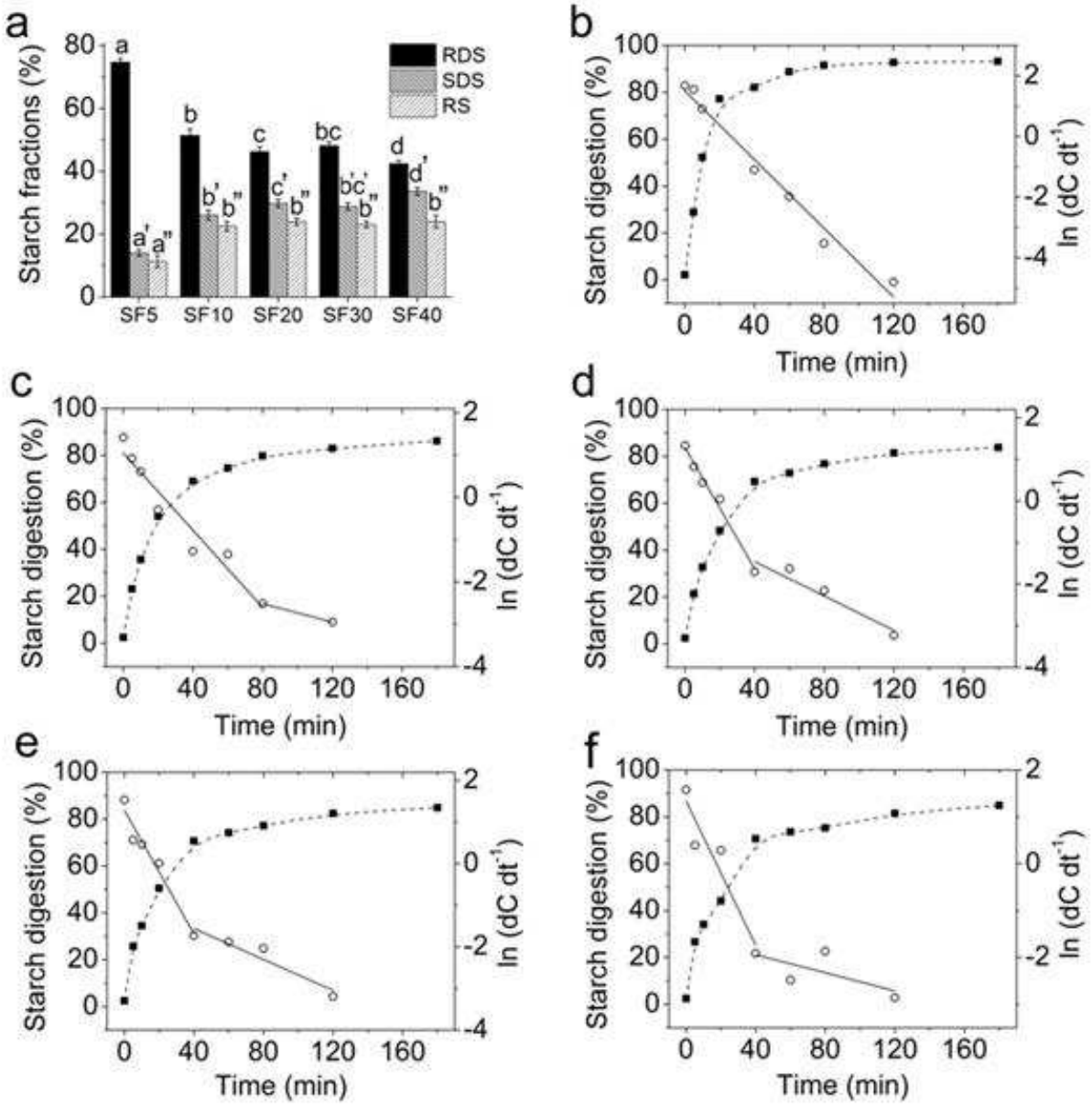

Fig. 4. Estimations of the RDS, SDS, and, RS using the Englyst method (a). [a, b, c]Different letters indicate significant difference within the group ($p < 0.05$, Tukey's HSD Post Hoc analysis). All RDS samples are depicted without a prime, SDS samples are depicted with ', and RS samples are depicted with ", for clarity (primes do not correspond to any statistical interpretation). The data for different groups were reported as the mean ± standard deviation (n = 3). Starch hydrolysis curve (■), model fitting (−), and LOS plots (○) of SF5 (b), SF10 (c), SF20 (d), SF30 (e), and SF40 (f).

Table 1. Digestion parameters.

		SF5	SF10	SF20	SF30	SF40
Phase I	k_1 (min^{-1})	0.052	0.055	0.059	0.060	0.059
	C_{t1} (%)	86	76	70	70	63
Phase II	k_2 (min^{-1})	ND	0.018	0.016	0.014	0.010
	C_{t2} (%)	ND	39	31	29	25

k_1 and k_2 are the rate constants for the first and second phases of digestion; C_{t1} and C_{t2} are the digested proportions of starch at the first and second phases of digestion. Values are means of experimental (n = 2) values. ND, not detected.

The SF5 (**Fig. 4b**) displayed a single-phase digestion behavior. For SF5, since the discotic stacking, and V and B-type packing order were not defined, the disordered-loosely packed and more mobile polymers (or random chains) were likely to bind easily to amylases for hydrolysis. Such a poorly defined molecular order in starch is known to be more susceptible to enzyme digestion [41]. For SF10, a slower digestion regime appeared after 80 min (**Fig. 4c**). In other words, SF10 showed an ability to resist digestion to some extent compared to SF5, although the samples did not reveal any stacking or mature packing order as discussed previously. However, we did observe the onset of chain ordering (cp. broad diffraction contribution for SF10 in **Fig. 3**) leading to imperfect packing registries. Imperfect registries are known to increase SDS content in starches [36]. Here, the chains should not be capable of pulling out of the registries as easily as SF5 for digestion by amylases. Interestingly, for SF20, SF30, and SF40, the polymers displayed a clear two-phase digestion process (**Fig. 4d-f**), pointing to the development of a secondary slower digestible phase. This is in agreement with the development of discotic stacking order in samples SF20, SF30, and SF40. Note that a development of V and B-type packing order was also

evidenced in the samples, SF20, SF30 and SF40 (**Fig. 3**). The V and B-type packing order are known to hinder starch digestion [42]. The samples were distinguished by independent rate constants (namely, k_1 and k_2). The kinetic parameters and corresponding $C_{t1, t2}$ are listed in **Table 1**. Here, the difference between k_1 and k_2 ($k_1 > k_2$, k_2 being ca. $^1/_3 \times k_1$ for the average of the samples, cp. **Table 1**) follows the order of SF40 > SF30 > SF20. As the increasing FA content leads to the development of discotic stacking and concomitant V and B-type packing order, polymer chains need to be pulled out of the ordered registries in order to be digested by amylases. Thus, increased order in the registries and increasing relative crystallinity reduce the fast digestion kinetics with the rate k_1. Remarkably, nearly 62 % (C_{t1}) of the polymer could be readily hydrolyzed at this fast rate i.e. k_1 (**Table 1**) in sample SF40 (**Fig. 4f**). Note that SF40 had the same packing order as SF20 and SF30, but, displayed higher crystallinity than the latter two. Since the amorphous fraction of SF40 was ca. 75 % (cp. crystallinity 25%), the digestion at the first phase is proposed to occur only in parts in the account of the amorphous matter. Although increased crystallinity in the samples can be attributed to the inhibited digestion, crystallinity cannot be therefore the sole measure of governing the resistance to starch digestion. Pu and coworkers [28] have also proposed that crystallinity is not the sole measure that dictates the resistance of starch to digestion. At the end of phase II, nearly 24 % (C_{t2}) of the remaining SF40 was hydrolyzed (**Table 1**). The D-spacing corresponding to ca. 27 nm amounts to the same size-order as that of the diameter of the digestive amylase enzyme. Such a structural feature of this magnitude has also been suggested earlier [27] to hinder starch digestibility. Similarly, D-spacing ca. 15-18 nm thickness (broad peak at q = 0.35-0.43 nm^{-1}) corresponds to a reduction in digestibility in hydrothermal-pressure treated corn starch [28]. Additionally, in our case, the development of the helical super-structures, forming microfibril-like anisotropic structures should

tightly bind unit cells housing the polymer chains. Such tight packing further ensures that the portions of polymer chains that are intimately associated in forming such registries are unlikely to extract and bind to the active site of digestive amylases.

The controls ACS, S/DMSO and S/DCC (**Fig. S4b-d**) displayed a dual-phase, the onset of dual-phase and a single phase digestion behavior, respectively. The kinetic parameters are provided in the **Table S1**.

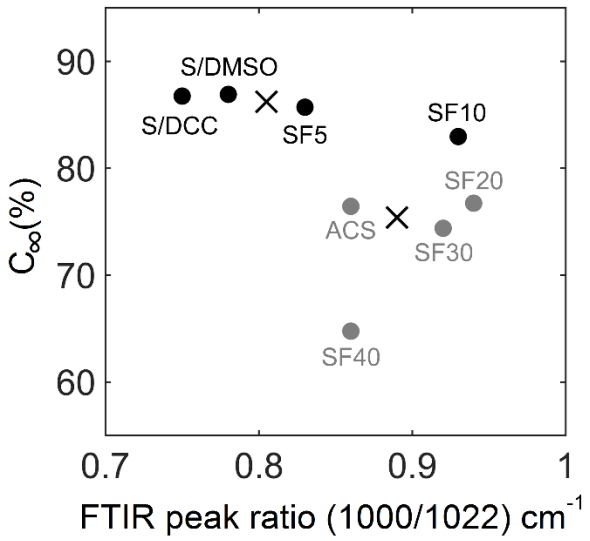

Fig. 5. The relationship between the total digestible starch (C_∞) and FTIR peak ratio (1000/1022) cm^{-1}, and, k-means cluster assignments and centroids (×). Here, black and grey markers indicate separate cluster assignments. All experimental points are presented as mean values.

To further investigate the order-digestion relationship, FTIR spectral peaks (1000 and 1022 cm^{-1}) were used to characterize the ordered and amorphous regions of the polymers, respectively. The peak ratio of 1000/1022 cm^{-1} was used as an indicator of the proportion of ordered to disordered chains [39]. As expected, the total amount of digestible starch (C_∞)

obtained from digestibility studies, decreased with the rise in FTIR 1000/1022 cm^{-1} peak ratio (**Fig. 5**). The SF5 with a relatively low peak ratio (0.83, i.e. lower ordered) had C_∞ values that were ca. 84% (calculated using equation (5)) of the total starch present in digestibility mixtures. On the contrary, for SF10 to SF30 (**Fig. 5**), esterification resulted in a decrease in C_∞, which corroborates with an increase in FTIR peak ratios. It is noteworthy, that the above relationship does not extend very far. The FTIR ratio decreased for SF40 as compared to SF10, SF20, and SF30, although a reduced digestion behavior has been observed for the former. This suggests that the decrease in the FTIR ratio does not correspond to a lower ordered polymer, but is attributed to an increase in liquid crystallinity instead. From the unsupervised k-means cluster analysis (**Fig. 5**), it is reasonable to state that structure dominated the digestion of the polymers, and a FA esterification at a crucial level of substitution of 0.04 (corresponding to SF20) or above was required to slow down the enzymatic hydrolysis of the polymer.

In summary, a molecular rearrangement of starch on esterification with FA results in the emergence of differing digestion rates of starch, k_1 and k_2 ($k_1 > k_2$). This implies that ordered polymers resulting from the FA-assisted discotic stacking, and V and B-type packing resisted hydrolysis of starch by α-amylase. The progressively diminishing k_2 rate values in samples SF10 to SF40 indicated that these ordering reduced the accessibility of the polymer to amylases, resulting in evidently reduced digestion extent (corresponding to decreased C_{t2}) in the second phase. The rate (k_2) was decreased ca. > 20%, and, > 15% (cp. **Table 1**) as the discotic stacking order matured in SF20 from SF10, and, in SF40 from SF30, respectively. Note that the V and B-type packing order was alike in the case of the latter. Therefore in relation to controlling digestion, we propose that the stacking order was a dominant feature over the packing order.

4. Conclusions

A combination of complementary techniques of scattering (small-angle X-ray scattering), diffraction (XRD), Fourier transform infrared (FTIR) spectroscopy, microscopy (bright-field and polarized) and in vitro digestion (classical Englyst digestion and kinetics) were assessed to probe the link between the structural evolution of amylopectin corn starch (ACS) on esterification with folic acid (FA) and its digestion rate. The mesoscopic order of the starch-folic acid ester (SF) derivatives were seen to be profoundly altered from random chains to the evolution of microfibril helices with strong optical anisotropy. The packing order also revealed the evolution of a V and B-type polymorphism. The SF exhibited the evolution of increased resistance to digestion, alongside the development of two independent rates of digestion (where $k_1 > k_2$). In the hierarchically ordered SF polymer, stacking over packing order was seen to be more influential in limiting the enzyme action, and, FA esterification at 0.04 level substitution (corresponding to SF20) or above was critical to slow down enzymatic hydrolysis of SF. These findings explain the structural mechanism behind how FA esterification can enable to control starch digestion kinetics. Therefore, the current results provide a solid platform for developing starch-folic acid esters as building-block copolymers for the design of smart, targeted starch-based oral delivery systems with tunable digestion for carrying pharmaceuticals and nutraceuticals.

Conflict of interest

The authors declare that they have no conflict of interest.

Acknowledgements

PKB is a Commonwealth Scholar funded by the UK government. Dr. Sally Boxal (Faculty of Biological Sciences, University of Leeds), Dr. Stephen Gorman (School of Chemistry, University of Leeds), Mr. Prakash Kurmi and Mr. Tridip Ranjan Nath (Sophisticated Analytical Instrumentation Centre, Tezpur University), and, Dr. Ratan Boruah and Mr. Biju Boro (Department of Physics, Tezpur University) are kindly acknowledged for their technical support in CLSM, FTIR, XRD and Polarized light microscopy, and, SEM, respectively. AS would sincerely thank Dr. Mel Holmes (School of Food Science and Nutrition, University of Leeds) for his proof-reading and editorial corrections. This work benefited from the use of the SasView application, originally developed under NSF Award DMR-0520547. SasView also contains code developed with funding from the EU Horizon 2020 programme under the SINE2020 project Grant No 654000.

References

[1] R. Khlibsuwan, W. Tansena, T. Pongjanyakul, Modification of alginate beads using gelatinized and ungelatinized arrowroot (Tacca leontopetaloides L. Kuntze) starch for drug delivery, Int. J. Biol. Macromol. 118 (2018) 683-692. https://doi.org/10.1016/j.ijbiomac.2018.06.118.

[2] H.E. Martinez-Flores, Y.K. Chang, F. Martinez-Bustos, V. Sgarbieri, Effect of high fiber products on blood lipids and lipoproteins in hamsters, Nutr. Res. 24 (2004) 85-93. https://doi.org/10.1016/j.nutres.2003.08.016.

[3] G. Baier, D. Baumann, J.r.M. Siebert, A. Musyanovych, V. Mailänder, K. Landfester, Suppressing unspecific cell uptake for targeted delivery using hydroxyethyl starch nanocapsules, Biomacromolecules 13 (2012) 2704-2715. https://doi.org/10.1021/bm300653v.

[4] S. Xiao, C. Tong, X. Liu, D. Yu, Q. Liu, C. Xue, D. Tang, L. Zhao, Preparation of folate-conjugated starch nanoparticles and its application to tumor-targeted drug delivery vector, Chinese Sci. Bull. 51 (2006) 1693-1697. https://doi.org/10.1007/s11434-006-2039-7.

[5] P.K. Borah, M. Rappolt, R.K. Duary, A. Sarkar, Effects of folic acid esterification on the hierarchical structure of amylopectin corn starch, Food Hydrocoll. 86 (2019) 162-171. https://doi.org/10.1016/j.foodhyd.2018.03.028.

[6] H.Z. Zhang, X.M. Li, F.P. Gao, L.R. Liu, Z.M. Zhou, Q.Q. Zhang, Preparation of folate-modified pullulan acetate nanoparticles for tumor-targeted drug delivery, Drug Deliv. 17 (1) (2010) 48-57. https://doi: 10.3109/10717540903508979.

[7] S. Pérez, E. Bertoft, The molecular structures of starch components and their contribution to the architecture of starch granules: A comprehensive review, Starch - Stärke 62 (2010) 389-420. https://doi.org/10.1002/star.201000013.

[8] W. Shi, Y. Wang, H. Zhang, Z. Liu, Z. Fei, Probing deep into the binding mechanisms of folic acid with α-amylase, pepsin and trypsin: An experimental and computational study, Food Chem. 226 (2017) 128-134. https://doi.org/10.1016/j.foodchem.2017.01.054.

[9] F. Zhu, Relationships between amylopectin internal molecular structure and physicochemical properties of starch, Trends Food Sci. Technol. 78 (2018) 234-242. https://doi.org/10.1016/j.tifs.2018.05.024.

[10] E. Bertoft, Understanding Starch Structure: Recent Progress, Agronomy 7(3) (2017) 56-85. https://doi.org/10.3390/agronomy7030056.

[11] Y. Patil-Sen, A. Sadeghpour, M. Rappolt, C.V. Kulkarni, Facile preparation of internally self-assembled lipid particles stabilized by carbon nanotubes, J. Vis. Exp. 108 (2016). https://doi.org/10.3791/53489.

[12] E. Adal, A. Sadeghpour, S.D.A. Connell, M. Rappolt, E. Ibanoglu, A. Sarkar, Heteroprotein complex formation of bovine lactoferrin and pea protein isolate: A multiscale structural analysis, Biomacromolecules 18 (2017) 625–635. https://doi.org/10.1021/acs.biomac.6b01857.

[13] V.P. Yuryev, A.V. Krivandin, V.I. Kiseleva, L.A. Wasserman, N.K. Genkina, J. Fornal, W. Blaszczak, A. Schiraldi, Structural parameters of amylopectin clusters and semi-crystalline growth rings in wheat starches with different amylose content, Carbohydr. Res. 339 (2004) 2683-2691. https://doi.org/10.1016/j.carres.2004.09.005.

[14] A. Mohamed, T. Ardyani, S.A. Bakar, M. Sagisaka, Y. Umetsu, J. Hamon, B.A. Rahim, S.R. Esa, H.A. Khalil, M.H. Mamat, Rational design of aromatic surfactants for graphene/natural rubber latex nanocomposites with enhanced electrical conductivity, J. Colloid Interface Sci. 516 (2018) 34-47. https://doi.org/10.1016/j.jcis.2018.01.041.

[15] M. Minekus, M. Alminger, P. Alvito, S. Ballance, T. Bohn, C. Bourlieu, F. Carriere, R. Boutrou, M. Corredig, D. Dupont, A standardised static in vitro digestion method suitable for

food–an international consensus, Food Funct. 5 (2014) 1113-1124. https://doi.org/10.1039/c3fo60702j.

[16] C. Gonçalves, R.M. Rodriguez-Jasso, N. Gomes, J.A. Teixeira, I. Belo, Adaptation of dinitrosalicylic acid method to microtiter plates, Anal. Methods 2 (2010) 2046-2048. https://doi.org/ 10.1039/C0AY00525H.

[17] I. Goñi, A. García-Alonso, F. Saura-Calixto, A starch hydrolysis procedure to estimate glycemic index, Nutr. Res. 17 (1997) 427-437. https://doi.org/10.1016/S0271-5317(97)00010-9.

[18] H.N. Englyst, S. Kingman, J. Cummings, Classification and measurement of nutritionally important starch fractions, Eur. J. Clin. Nutr. 46 (1992) S33-50. Suppl 2.

[19] P.J. Butterworth, F.J. Warren, T. Grassby, H. Patel, P.R. Ellis, Analysis of starch amylolysis using plots for first-order kinetics, Carbohydr. Polym. 87 (2012) 2189-2197. https://doi.org/10.1016/j.carbpol.2011.10.048.

[20] B.R. Poulsen, G. Ruiter, J. Visser, J.J.L. Iversen, Determination of first order rate constants by natural logarithm of the slope plot exemplified by analysis of Aspergillus niger in batch culture, Biotechnol. Lett. 25 (2003) 565-571. https://doi.org/10.1023/A:1022836815439.

[21] T. Kanungo, D.M. Mount, N.S. Netanyahu, C.D. Piatko, R. Silverman, A.Y. Wu, An efficient k-means clustering algorithm: analysis and implementation, IEEE Trans. Pattern Anal. Mach. Intell. 24 (2002) 881-892. https://doi.org/10.1109/TPAMI.2002.1017616.

[22] S. Bonazzi, M.M. DeMorais, G. Gottarelli, P. Mariani, G.P. Spada, Self-assembly and liquid crystal formation of folic acid salts, Angew Chem. Int. Ed. 32 (1993) 248-250. https://doi.org/10.1002/anie.199302481.

[23] Y. Kamikawa, M. Nishii, T. Kato, Self-Assembly of Folic Acid Derivatives: Induction of Supramolecular Chirality by Hierarchical Chiral Structures, Chem. Eur. J. 10 (2004) 5942-5951. https://doi.org/10.1002/chem.200400424.

[24] J. Zhu, X. Li, C. Huang, L. Chen, L. Li, Structural changes and triacetin migration of starch acetate film contacting with distilled water as food simulant, Carbohydr. Polym 104 (2014) 1-7. https://doi.org/10.1016/j.carbpol.2013.12.087.

[25] J. Zhu, X. Li, C. Huang, L. Chen, L. Li, Plasticization effect of triacetin on structure and properties of starch ester film, Carbohydr. Polym. 94 (2013) 874-881. https://doi.org/10.1016/j.carbpol.2013.02.020.

[26] X. Shen, W. Shang, P. Strappe, L. Chen, X. Li, Z. Zhou, C. Blanchard, Manipulation of the internal structure of high amylose maize starch by high pressure treatment and its diverse influence on digestion, Food Hydrocoll. 77 (2018) 40-48. https://doi.org/10.1016/j.foodhyd.2017.09.015.

[27] T. Suzuki, A. Chiba, T. Yarno, Interpretation of small angle x-ray scattering from starch on the basis of fractals, Carbohydr. Polym. 34 (1997) 357-363. https://doi.org/10.1016/S0144-8617(97)00170-7.

[28] H. Pu, L. Chen, L. Li, X. Li, Multi-scale structural and digestion resistibility changes of high-amylose corn starch after hydrothermal-pressure treatment at different gelatinizing temperatures, Food Res. Int. 53 (2013) 456-463. https://doi.org/10.1016/j.foodres.2013.05.021.

[29] O. Kratky, G. Porod, Röntgenuntersuchung gelöster Fadenmoleküle, Recl. Trav. Chim. Pays-Bas 68 (1949) 1106-1122. https://doi.org/10.1002/recl.19490681203.

[30] C. Tschierske, Materials chemistry: Liquid crystals stack up, Nature 419 (2002) 681. https://doi.org/10.1038/419681a.

[31] G. Pelzl, S. Diele, W. Weissflog, Banana-shaped compounds—a new field of liquid crystals, Adv. Mater. 11 (1999) 707-724. https://doi.org/10.1002/(SICI)1521-4095(199906)11:9<707::AID-ADMA707>3.0.CO;2-D.

[32] B. Zhang, Y. Zhao, X. Li, L. Li, F. Xie, L. Chen, Supramolecular structural changes of waxy and high-amylose cornstarches heated in abundant water, Food Hydrocoll. 35 (2014) 700-709. https://doi.org/10.1016/j.foodhyd.2013.08.028.

[33] G. Tawil, A. Viksø-Nielsen, A. Rolland-Sabaté, P. Colonna, A. Buléon, In depth study of a new highly efficient raw starch hydrolyzing α-amylase from Rhizomucor sp, Biomacromolecules 12 (2010) 34-42. https://doi.org/10.1021/bm100913z.

[34] S. Zabar, U. Lesmes, I. Katz, E. Shimoni, H. Bianco-Peled, Structural characterization of amylose-long chain fatty acid complexes produced via the acidification method, Food Hydrocoll. 24 (2010) 347-357. https://doi.org/10.1016/j.foodhyd.2009.10.015.

[35] M.C. Godet, V. Tran, M.M. Delage, A. Buléon, Molecular modelling of the specific interactions involved in the amylose complexation by fatty acids, Int. J. Biol. Macromol. 15 (1993) 11-16. https://doi.org/10.1016/S0141-8130(05)80082-0.

[36] P.K. Borah, S.C. Deka, R.K. Duary, Effect of repeated cycled crystallization on digestibility and molecular structure of glutinous Bora rice starch, Food Chem. 223 (2017) 31-39. https://doi.org/10.1016/j.foodchem.2016.12.022.

[37] A. Imberty, S. Perez, A revisit to the three-dimensional structure of B-type starch, Biopolymers. 27 (1988) 1205-1221. https://doi.org/10.1002/bip.360270803.

[38] A. Vora, A. Riga, D. Dollimore, K.S. Alexander, Thermal stability of folic acid, Thermochim. Acta 392-393 (2002) 209-220. https://doi.org/10.1016/S0040-6031(02)00103-X.

[39] H. Patel, R. Day, P.J. Butterworth, P.R. Ellis, A mechanistic approach to studies of the possible digestion of retrograded starch by α-amylase revealed using a log of slope (LOS) plot, Carbohydr. Polym. 113 (2014) 182-188. https://doi.org/10.1016/j.carbpol.2014.06.089.

[40] D. Qiao, F. Xie, B. Zhang, W. Zou, S. Zhao, M. Niu, R. Lv, Q. Cheng, F. Jiang, J. Zhu, A further understanding of the multi-scale supramolecular structure and digestion rate of waxy starch, Food Hydrocoll. 65 (2017) 24-34. https://doi.org/10.1016/j.foodhyd.2016.10.041.

[41] D. Gallant, B. Bouchet, A. Buleon, S. Perez, Physical characteristics of starch granules and susceptibility to enzymatic degradation, Eur. J. Clin. Nutr. 46 (1992) 3-16. Suppl 2.

[42] S. Dhital, F.J. Warren, P.J. Butterworth, P.R. Ellis, M.J. Gidley, Mechanisms of starch digestion by α-amylase—Structural basis for kinetic properties, Crit. Rev. Food Sci. Nutr. 57 (2017) 875-892. https://doi.org/10.1080/10408398.2014.922043.

Highlights

- Esterification with folic acid results in a hierarchical re-structuring of starch
- Relationship exists between structural evolution and rate of digestion
- Starch with higher folic acid esterification displays two digestion rates ($k_1 > k_2$)
- The stacking order impacts the starch digestion more than the packing order
- Esterification of starch with folic acid is a new tool to tailor starch digestion